

# Near-Field Source Localization in 3-D Using Two Parallel Centrally Symmetric Unfold Coprime Array

Hua Chen<sup>1</sup>, Senior Member, IEEE, Junjie Li<sup>1</sup>, Songjie Yang<sup>1</sup>, Wei Liu<sup>2</sup>, Senior Member, IEEE, Yonina C. Eldar<sup>3</sup>, Fellow, IEEE, and Chau Yuen<sup>4</sup>, Fellow, IEEE

**Abstract**—Most near-field (NF) localization algorithms cannot deal with the underdetermined case, while those which can are computationally expensive due to employment of fourth-order cumulants. In this work, a low-complexity solution is provided for underdetermined three-dimensional (3-D) NF localization, by employing second-order statistics with a tailored array configuration named two parallel centrally symmetric unfold coprime (TPSC) array. Its implementation can be divided into three stages. Firstly, the proposed algorithm constructs two cross-correlation matrices based on the received array data, which eliminates the non-linear range-related information of NF signals. Secondly, covariance and vectorization operations are applied to these two cross-correlation matrices to form a virtual array with extended aperture. Finally, the two-dimensional (2-D) angle parameters are estimated by the sparse and parametric approach (SPA) and a phase retrieval operation, and then the one-dimensional (1-D) range parameter is achieved by the multiple signal classification (MUSIC) algorithm. One specific feature is that the estimated angle and range parameters are matched automatically. An analysis of the properties of the TPSC array is provided, and an optimal parameter configuration is derived, given that the total number of array elements is fixed. Simulation results demonstrate that the designed TPSC array can achieve underdetermined 3-D NF localization, and deliver enhanced estimation capabilities, surpassing those of established algorithms.

**Index Terms**—Near-field, coprime array, symmetric array, underdetermined case, source localization.

## I. INTRODUCTION

**S**OURCE localization, a significant topic in array signal processing, has been extensively studied across various applications, including radar, sonar, and wireless communications [1], [2], [3], [4], [5], [6]. According to the distance between the target signal and the array [7], [8], source localization can be divided into far-field (FF) source localization and near-field (NF) source localization. When the distance between the source and the array is sufficiently large, resulting in the source being situated within the FF region, the propagation delays of the FF sources are characterized by the direction-of-arrival (DOA) parameter. When the sources are situated close to the array and reside within the NF region, the impinging signals behave as spherical waves. Consequently, the NF signals are characterized by two distinct parameters: DOA and range, which renders many FF localization techniques inapplicable to NF.

With advancements in wireless communication systems, particularly the increasing array aperture, NF signal processing has garnered substantial attention due to its ability to provide more accurate channel models. Consequently, numerous new techniques related to NF localization have been developed, such as NF beam training [9], [10] and NF channel estimation [11], [12], [13]. These advancements underscore the significance of NF signal processing. One approach to increase the array aperture is the utilization of sparse linear arrays (SLAs) for NF source localization [14], [15], [16], [17], [18], [19], [20], [21]. Compared to uniform linear arrays (ULAs), SLAs [22], [23], [24], [25], [26], [27] offer a larger physical aperture and more degrees of freedom (DOFs) for a given number of elements, and therefore play an essential role for underdetermined direction of arrival estimation.

For SLA-based NF source localization in [14], an algorithm based on a sparse symmetric array is presented, leveraging a hybrid-order multiple signal classification (MUSIC) algorithm to process the cumulant matrix obtained from the array, and thereby estimating the required angle and range parameters. With partial knowledge of calibration sources, an iterative self-calibration algorithm is introduced in [15], facilitating concurrent estimation of gain and phase error parameters, as well as source parameters. In [16], a parameter estimation method for NF sources using symmetric nested array (SNA) is suggested, where the application of fourth-order cumulants in the received data allows the SNA to form at least  $4N + 4MN - 2M - 3$  continuous segments with only

Received 6 July 2024; revised 25 December 2024 and 7 February 2025; accepted 13 February 2025. Date of publication 26 February 2025; date of current version 12 June 2025. This work was supported in part by Zhejiang Provincial Natural Science Foundation of China under Grant LY23F010003 and Grant LR20F010001; in part by the ‘‘Pioneer’’ and ‘‘Leading Goose’’ Research and Development Program of Zhejiang Province under Grant 2024C01105; in part by the National Natural Science Foundation of China under Grant U24A20217 and Grant 62001256; in part by U.K. Engineering and Physical Sciences Research Council (EPSRC) under Grant EP/V009419/2; in part by Singapore Ministry of Education (MOE) Tier 2 under Grant MOE-T2EP50220-0019; in part by the National Research Foundation, Singapore, and Infocomm Media Development Authority under its Future Communications Research and Development Programme under Grant FCP-NTU-RG-2024-025; and in part by China Scholarship Council under Grant 202408330215 and Grant 202306070094. The associate editor coordinating the review of this article and approving it for publication was A. G. Kanatas. (Corresponding author: Hua Chen.)

Hua Chen and Junjie Li are with the Faculty of Electrical Engineering and Computer Science, Ningbo University, Ningbo 315211, China (e-mail: dkchenhua0714@hotmail.com).

Songjie Yang is with the National Key Laboratory of Wireless Communications, University of Electronic Science and Technology of China, Chengdu 610054, China (e-mail: yangsongjie@std.uestc.edu.cn).

Wei Liu is with the Department of Electrical and Electronic Engineering, The Hong Kong Polytechnic University, Hong Kong (e-mail: wei2.liu@polyu.edu.hk).

Yonina C. Eldar is with the Faculty of Mathematics and Computer Science, Weizmann Institute of Science, Rehovot 7610001, Israel (e-mail: yonina.eldar@weizmann.ac.il).

Chau Yuen is with the School of Electrical and Electronic Engineering, Nanyang Technological University, Singapore 639798 (e-mail: chau.yuen@ntu.edu.sg).

Digital Object Identifier 10.1109/TWC.2025.3543616

$2M + 2N - 1$  sensors ( $M$  and  $N$  are integers, with  $N > 1$  and  $M > 0$ ). Based on a symmetric linear array in [17], oblique projection techniques are applied to separate NF sources from mixed near and FF sources. Atomic norm minimization is then used for angle parameter estimation, followed by range parameter estimation using a one-dimensional (1-D) search method. In [18], a convolutional neural network (CNN) is proposed to transform the received data from time domain to frequency domain, employing CNN and autoencoder to separate and locate the mixed sources. A symmetric displaced coprime array (SDCA) is employed in [19], composed of three SLAs, with the same number of array elements, which can provide a larger array aperture and a wider range of continuous segments than SNA in [16]. In [20], angle and range parameters are estimated through spatial smoothing and the MUSIC algorithm, utilizing a symmetric extended nested array (SENA) built upon the foundation developed from the compressed symmetric nested array (CSNA). With the optimization of array configuration parameters, SENA exhibits larger physical aperture, longer continuous segments, and better estimation performance than existing symmetric sparse arrays. Also based on SLA, a NF source localization algorithm is introduced in [21], leveraging the structure of a coprime array. The method first constructs an off-grid model which solely contains angle parameter, and subsequently, an iterative approach is employed for estimating the 1-D angle parameter, which are then substituted into the range parameter model for iteratively estimating the range parameter.

Although the above algorithms based on SLA yield excellent performance in parameter estimation, they are limited to two-dimensional (2-D) parameter estimation for the NF signals case, namely, the 1-D azimuth and range. In practice, it is often desirable to locate NF targets in three-dimensional (3-D) space with planar arrays, which involves estimating azimuth, elevation, and range parameters, thereby posing a more intricate challenge in parameter pairing.

To enable 3-D parameter estimation for NF signals, various arrays have been proposed, such as cross arrays, uniform circular arrays, and rectangular arrays. As a representative example, a gridless NF source localization algorithm is proposed based on a cross array in [28], which constructs a sparse model to transform the parameter estimation problem into a semi-positive definite programming (SDP) problem. In [29], a uniform circular array is suggested utilizing a joint phase interferometer and the MUSIC algorithm. A NF source localization algorithm for uniform rectangular array (URA) or centrally symmetric sparse rectangular array (SRA) is developed in [30] which utilizes fourth-order cumulants to convert the angle estimation problem into a low-rank reconstruction problem, and achieve range estimation using a 1-D MUSIC algorithm. Similar to [28], cross array is also used in [31] for NF source localization, yet without resorting to the Fresnel approximation. Accounting for disparate propagation attenuation across sensors, the algorithm constructs a third-order parallel factor (PARAFAC) data model, and then the parameters are estimated through trilinear decomposition and a least squares method.

In recent study of nonuniform cross arrays, fourth-order cumulants matrices and vectorization operations are employed in [32], effectively achieving underdetermined estimation for

2-D angle and range parameters of NF sources. Although the aforementioned algorithms are capable of achieving NF source localization, they cannot work in the underdetermined case (except for Ref. [32]). Research into underdetermined estimation algorithms for array processing is instrumental in reducing the cost associated with a large number of array elements.

In summary, existing NF algorithms can be categorized into three types: the first type ([14], [15], [16], [17], [18], [19], [20], [21]) offers high accuracy in parameter estimation but is limited to the 2-D plane scene; the second type ([28], [28], [29], [30], [31]) achieves 3-D parameter estimation but lacks the capability for underdetermined estimation; the third type ([32]), though capable of underdetermined estimation, relies on fourth-order cumulants, resulting in high computational complexity. These challenges underscore the pressing need for low-complexity solutions for underdetermined 3-D NF estimation.

In this paper, we propose an algorithm based on a two parallel centrally symmetric unfold coprime (TPSC) array for underdetermined localization of NF sources. Based on the special array structure, the proposed algorithm eliminates the non-linear range-related information in the phase part of the steering matrix by constructing two cross-correlation matrices. Subsequently, it enlarges the array aperture through covariance and vectorization operations. Finally, the NF signals' 3-D parameters are estimated using the sparse and parametric approach (SPA) [33] and the 1-D MUSIC algorithm.

The main contributions of this paper are as follows:

1) A TPSC array is proposed, which unfolds the coprime array and introduces central symmetry, facilitating elimination of the nonlinear range-related information inherent in the phase component of the steering matrix for NF signals. An analysis of the TPSC array's properties is provided, followed by proposition of the optimal parameter configuration for the proposed TPSC array.

2) The cross-correlation calculation is utilized to construct two matrices followed by vectorization, which expands the virtual array aperture, enhancing the parameter estimation performance. Simulation results show the proposed algorithm's superiority in terms of estimation accuracy, underdetermined and mixed source estimation abilities.

Notations:  $(\cdot)^*$ ,  $(\cdot)^T$ ,  $(\cdot)^\dagger$ , and  $(\cdot)^H$  respectively denote the operations of conjugation, transpose, pseudo-inverse, and conjugate transpose;  $E\{\cdot\}$  represents the mathematical expectation;  $\odot$  denotes the Khatri-Rao product;  $\text{vec}(\cdot)$  represents vectorization;  $\text{diag}(\cdot)$  stands for diagonalization;  $\text{undia}(\cdot)$  represents diagonal extraction;  $\text{angle}(\cdot)$  gives the the phase/angle of a complex number, and  $\text{tr}(\cdot)$  represents the trace of a matrix.

## II. PROPOSED TPSC ARRAY

Consider an NF scenario in which  $K$  narrowband NF sources are uniquely described by the 3-D parameters: azimuth  $\varphi_k$ , elevation  $\theta_k$ , and range  $r_k$ , as shown in Fig. 1, where  $k = 1, 2, \dots, K$ . The  $xoy$  plane of the coordinate system is populated with sensors, where the sensor at origin is set as the reference. The unit length along all axes within the coordinate

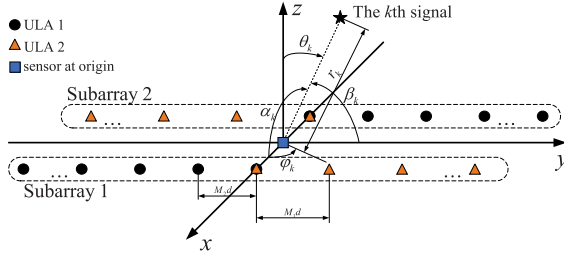


Fig. 1. The two parallel centrally symmetric unfold coprime array structure.

system is defined as  $d$ , where  $d = \lambda/4$  and  $\lambda$  represents the signal wavelength. Specifically, for a sensor located at  $(m, n)$  in the  $xoy$  plane, the received signal is modeled as follows

$$x_{m,n}(t) = \sum_{k=1}^K s_k(t) e^{j\tau_{m,n}(k)} + v_{m,n}(t) \quad (1)$$

where  $s_k(t)$  is the NF signals and  $v_{m,n}(t)$  denotes the additive white Gaussian noise. The  $k$ -th signal's path delay with respect to the sensor located at  $(m, n)$  is  $\tau_{m,n}(k)$ , which can be expressed as

$$\tau_{m,n}(k) = \frac{2\pi}{\lambda} [r_{m,n}(k) - r_k] \quad (2)$$

where  $r_{m,n}(k)$  is the range from the sensor located at  $(m, n)$  to the  $k$ -th signal and  $r_k$  is the range from coordinate origin to the  $k$ -th signal. By geometric principles as (3), shown at the bottom of the page.

Applying the Fresnel approximation [34], [35], [36] to  $r_{m,n}(k)$  and substituting it into (2), we obtain the following expression

$$\tau_{m,n}(k) \approx \omega_{kx}m + \phi_{kx}m^2 + \omega_{ky}n + \phi_{ky}n^2 + \mu_k \quad (4)$$

where

$$\omega_{kx} = \frac{-2\pi d \sin\theta_k \cos\varphi_k}{\lambda} = \frac{-2\pi d \cos\alpha_k}{\lambda} \quad (5)$$

$$\phi_{kx} = \frac{\pi d^2 (1 - \sin^2\theta_k \cos^2\varphi_k)}{\lambda r_k} = \frac{\pi d^2 \sin^2\alpha_k}{\lambda r_k} \quad (6)$$

$$\omega_{ky} = \frac{-2\pi d \sin\theta_k \sin\varphi_k}{\lambda} = \frac{-2\pi d \cos\beta_k}{\lambda} \quad (7)$$

$$\phi_{ky} = \frac{\pi d^2 (1 - \sin^2\theta_k \sin^2\varphi_k)}{\lambda r_k} = \frac{\pi d^2 \sin^2\beta_k}{\lambda r_k} \quad (8)$$

$$\mu_k = \frac{-\pi d^2 \sin^2\theta_k \sin 2\varphi_k}{\lambda r_k} = \frac{-2\pi d^2 \cos\alpha_k \cos\beta_k}{\lambda r_k} \quad (9)$$

In (5)-(9), we transform the challenge of solving for angles  $\theta_k$  and  $\varphi_k$  into angles  $\alpha_k$  and  $\beta_k$ . Consequently, (1) can be reformulated as

$$\begin{aligned} x_{m,n}(t) &= \sum_{k=1}^K s_k(t) e^{j[\omega_{kx}m + \phi_{kx}m^2 + \omega_{ky}n + \phi_{ky}n^2 + \mu_k]} + v_{m,n}(t). \end{aligned} \quad (10)$$

As indicated by (10), the 3-D parameter estimation problem is fundamentally nonlinear, arising from the exponential term involving range-related nonlinear information such as  $\phi_{kx}$  and  $\phi_{ky}$ . To counteract this challenge, we design the TPSC array and apply cross-correlation calculations to the received data, effectively eliminating the undesirable nonlinear components.

The TPSC model consists of two subarrays and one sensor set at origin, where subarray 1 and subarray 2 have identical configurations and exhibit centrosymmetry about the origin. Each subarray consists of two ULAs, denoted as ULA 1 and ULA 2. The number of elements in ULA 1 and ULA 2 are  $M_1$  and  $M_2$ , respectively, where  $M_1$  and  $M_2$  are coprime integers with  $M_1 > M_2$ . ULA 1 and ULA 2 share elements on the  $x$ -axis. The received data can be respectively represented as

$$\mathbf{x}_1(t) = \mathbf{A}_1(\alpha, \beta, r)\mathbf{s}(t) + \mathbf{n}_1(t) \quad t \in [L] \quad (11)$$

$$\mathbf{x}_2(t) = \mathbf{A}_2(\alpha, \beta, r)\mathbf{s}(t) + \mathbf{n}_2(t) \quad t \in [L] \quad (12)$$

$$x_3(t) = \sum_{k=1}^K s_k(t) + n_3(t) \quad t \in [L] \quad (13)$$

where  $t$  is the snapshot index and  $L$  is the number of snapshots. Here,  $\mathbf{x}_1(t) = [x_{1,1}(t), x_{1,2}(t), \dots, x_{1,(M_1+M_2-1)}(t)]^T$ ,  $\mathbf{x}_2(t) = [x_{2,1}(t), x_{2,2}(t), \dots, x_{2,(M_1+M_2-1)}(t)]^T$ , and  $x_3(t)$  is the received data of the element at the origin, with  $x_{1,a}(t)$  and  $x_{2,b}(t)$  denoting the received data of the  $a$ th element in subarray 1 and the  $b$ th element in subarray 2 ( $a, b \in [1, M_1 + M_2 - 1]$ ), respectively.  $\mathbf{A}_1(\alpha, \beta, r) = [\mathbf{a}_1(\alpha_1, \beta_1, r_1), \mathbf{a}_1(\alpha_2, \beta_2, r_2), \dots, \mathbf{a}_1(\alpha_K, \beta_K, r_K)] \in \mathbb{C}^{(M_1+M_2-1) \times K}$ ,  $\mathbf{A}_2(\alpha, \beta, r) = [\mathbf{a}_2(\alpha_1, \beta_1, r_1), \mathbf{a}_2(\alpha_2, \beta_2, r_2), \dots, \mathbf{a}_2(\alpha_K, \beta_K, r_K)] \in \mathbb{C}^{(M_1+M_2-1) \times K}$  are the steering matrices of the subarrays with each element in the corresponding column being  $a_{1m}(\alpha_k, \beta_k, r_k) = e^{-j\tau_{1m,k}}$ ,  $a_{2n}(\alpha_k, \beta_k, r_k) = e^{-j\tau_{2n,k}}$ , where  $1 \leq m, n \leq (M_1+M_2-1)$ , and  $\tau_{1m,k}$  and  $\tau_{2n,k}$  respectively represent the propagation delays associated with the  $m$ th element in subarray 1 and  $n$ th element in subarray 2.  $\mathbf{s}(t) = [s_1(t), s_2(t), \dots, s_K(t)]^T$  is the signal vector, and  $\mathbf{n}_1(t)$ ,  $\mathbf{n}_2(t)$ ,  $n_3(t)$  denote the additive white Gaussian noise of the corresponding subarrays. For convenience, the steering matrices of subarrays 1 and 2 are simplified into  $\mathbf{A}_1$  and  $\mathbf{A}_2$ .

Define  $\Omega_1 = [\Omega_{1,1}, \Omega_{1,2}, \dots, \Omega_{1,(M_1+M_2-1)}]$  and  $\Omega_2 = [\Omega_{2,1}, \Omega_{2,2}, \dots, \Omega_{2,(M_1+M_2-1)}]$  as the sets of  $y$ -coordinate values of all elements in subarray 1 and subarray 2, respectively, where  $(0.5, \Omega_{1,a}, 0)$  and  $(-0.5, \Omega_{2,b}, 0)$  denote the coordinate of the  $a$ th element in subarray 1 and the  $b$ th element in subarray 2 ( $a, b \in [1, M_1 + M_2 - 1]$ ). Due to the centrosymmetric property of subarray 1 and subarray 2 with respect to the origin, we have  $\Omega_{1,a} = -\Omega_{2,b}$ , where  $a + b = M_1 + M_2$ .

Considering the  $k$ th column of  $\mathbf{A}_1$  and  $\mathbf{A}_2$ , we have

$$\begin{aligned} \mathbf{a}_1(\alpha_k, \beta_k, r_k) &= [e^{-j[0.5\omega_{kx} + 0.5^2\phi_{kx} + \Omega_{1,1}\omega_{ky} + \Omega_{1,1}^2\phi_{ky} + 0.5\Omega_{1,1}\mu_k]}] \end{aligned}$$

$$r_{m,n}(k) = \sqrt{(r_k \sin\theta_k \cos\varphi_k - md)^2 + (r_k \sin\theta_k \sin\varphi_k - nd)^2 + (r_k \sin\theta_k)^2} \quad (3)$$

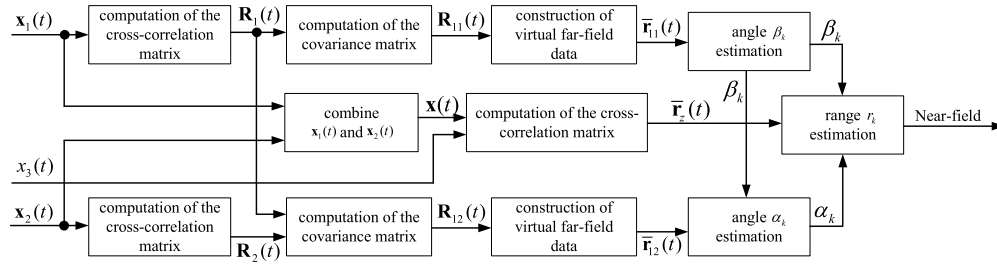


Fig. 2. The simplified flowchart of the proposed algorithm.

$$e^{-j[0.5\omega_{kx}+0.5^2\phi_{kx}+\Omega_{1,2}\omega_{ky}+\Omega_{1,2}^2\phi_{ky}+0.5\Omega_{1,2}\mu_k]}, \dots, e^{-j[0.5\omega_{kx}+0.5^2\phi_{kx}+\Omega_{1,P}\omega_{ky}+\Omega_{1,P}^2\phi_{ky}+0.5\Omega_{1,P}\mu_k]}], \quad (14)$$

and

$$\mathbf{a}_2(\alpha_k, \beta_k, r_k) = [e^{-j[-0.5\omega_{kx}+0.5^2\phi_{kx}+\Omega_{2,1}\omega_{ky}+\Omega_{2,1}^2\phi_{ky}-0.5\Omega_{2,1}\mu_k]}, e^{-j[-0.5\omega_{kx}+0.5^2\phi_{kx}+\Omega_{2,2}\omega_{ky}+\Omega_{2,2}^2\phi_{ky}-0.5\Omega_{2,2}\mu_k]}, \dots, e^{-j[-0.5\omega_{kx}+0.5^2\phi_{kx}+\Omega_{2,P}\omega_{ky}+\Omega_{2,P}^2\phi_{ky}-0.5\Omega_{2,P}\mu_k]}], \quad (15)$$

where the parameter  $P$  in  $\Omega_{1,P}$  and  $\Omega_{2,P}$  is equal to  $M_1 + M_2 - 1$ ,  $\omega_{kx} = -2\pi d \cos(\alpha_k)/\lambda$ ,  $\phi_{kx} = \pi d^2 \sin^2(\alpha_k)/\lambda r_k$ ,  $\omega_{ky} = -2\pi d \cos(\beta_k)/\lambda$ ,  $\phi_{ky} = \pi d^2 \sin^2(\beta_k)/\lambda r_k$ , and  $\mu_k = -2\pi d^2 \cos(\alpha_k) \cos(\beta_k)/\lambda r_k$ .

As the range parameter is taken to  $+\infty$ , the steering vector of the NF model in (14) and (15) will degenerate to that of the FF one, in which the proposed method can still work, as shown in Sec. V-F.

### III. THE PROPOSED ALGORITHM

This section presents an algorithmic flow where, starting from the data in (11), (12) and (13), cross-correlation matrices in (30) and (31) are constructed, which serve to form virtual FF data in (36) and (37), respectively. Then, SPA is used for sparse recovery in (39) to determine the angle  $\beta_k$ , followed by phase retrieval to obtain the angle  $\alpha_k$ . Finally, the MUSIC algorithm is applied to (49) to estimate the range  $r_k$ . The proposed algorithm is illustrated in the flowchart shown in Fig. 2, providing a clear visualization of its procedural steps.

#### A. Construction of Cross-Correlation Matrices

In this part, we construct two cross-correlation matrices using the data received by subarray 1 and subarray 2. The expressions for two collections of spatial-domain correlations at lag  $\tau$  are given as

$$r_{x_{2,l},x_{1,G-l}}(\tau) = E\{x_{2,l}(t+\tau)x_{1,G-l}^*(t)\} = \sum_{k=1}^K r_{sk}(\tau) e^{j(\omega_{kx} - 2\Omega_{2,l}\omega_{ky})} \quad (16)$$

$$r_{x_{1,l},x_{2,G-l}}(\tau) = E\{x_{1,l}(t+\tau)x_{2,G-l}^*(t)\} = \sum_{k=1}^K r_{sk}(\tau) e^{j(-\omega_{kx} - 2\Omega_{1,l}\omega_{ky})} \quad (17)$$

where  $G = M_1 + M_2$ , and  $r_{sk}(\tau) = E\{s_k(t+\tau)s_k^*(t)\}$ ,  $l = 1, 2, \dots, (M_1 + M_2 - 1)$ ,  $\tau \in N$ , with  $N$  representing the number of pseudo snapshots. Arranging  $r_{x_{2,l},x_{1,G-l}}(\tau)$  and  $r_{x_{1,l},x_{2,G-l}}(\tau)$  according to  $l$  allows the creation of two column vectors, denoted as  $\mathbf{r}_1(\tau)$  and  $\mathbf{r}_2(\tau)$ :

$$\mathbf{r}_1(\tau) = [r_{x_{2,1},x_{1,G-1}}(\tau), r_{x_{2,2},x_{1,G-2}}(\tau), \dots, r_{x_{2,G-1},x_{1,1}}(\tau)]^T \quad (18)$$

$$\mathbf{r}_2(\tau) = [r_{x_{1,1},x_{2,G-1}}(\tau), r_{x_{1,2},x_{2,G-2}}(\tau), \dots, r_{x_{1,G-1},x_{2,1}}(\tau)]^T \quad (19)$$

Next,  $\mathbf{r}_1(\tau)$  and  $\mathbf{r}_2(\tau)$  can be written as

$$\mathbf{r}_1(\tau) = \mathbf{B}_1 \Phi \mathbf{r}_s(\tau) \quad (20)$$

$$\mathbf{r}_2(\tau) = \mathbf{B}_2 \Phi^* \mathbf{r}_s(\tau) \quad (21)$$

where

$$\mathbf{B}_1 = [\mathbf{b}_1(\omega_{1y}), \mathbf{b}_1(\omega_{2y}), \dots, \mathbf{b}_1(\omega_{Ky})] \quad (22)$$

$$\mathbf{B}_2 = [\mathbf{b}_2(\omega_{1y}), \mathbf{b}_2(\omega_{2y}), \dots, \mathbf{b}_2(\omega_{Ky})] \quad (23)$$

$$\mathbf{b}_1(\omega_{ky}) = [e^{-2j\Omega_{2,1}\omega_{ky}}, e^{-2j\Omega_{2,2}\omega_{ky}}, \dots, e^{-2j\Omega_{2,(M_1+M_2-1)}\omega_{ky}}]^T \quad (24)$$

$$\mathbf{b}_2(\omega_{ky}) = [e^{-2j\Omega_{1,1}\omega_{ky}}, e^{-2j\Omega_{1,2}\omega_{ky}}, \dots, e^{-2j\Omega_{1,(M_1+M_2-1)}\omega_{ky}}]^T \quad (25)$$

$$\Phi = \text{diag}([e^{j\omega_{1x}}, e^{j\omega_{2x}}, \dots, e^{j\omega_{Kx}}]) \quad (26)$$

$$\mathbf{r}_s(\tau) = [r_{s1}(\tau), r_{s2}(\tau), \dots, r_{sK}(\tau)]^T \quad (27)$$

where  $\mathbf{B}_1$  and  $\mathbf{B}_2$  are both  $(M_1 + M_2 - 1) \times K$  matrices. By collecting  $N$  pseudo snapshots, we have

$$\mathbf{R}_1 = [\mathbf{r}_1(1), \mathbf{r}_1(2), \dots, \mathbf{r}_1(N)] \quad (28)$$

$$\mathbf{R}_2 = [\mathbf{r}_2(1), \mathbf{r}_2(2), \dots, \mathbf{r}_2(N)], \quad (29)$$

with

$$\mathbf{R}_1 = \mathbf{B}_1 \Phi \mathbf{R}_s \quad (30)$$

$$\mathbf{R}_2 = \mathbf{B}_2 \Phi^* \mathbf{R}_s \quad (31)$$

and  $\mathbf{R}_1$  and  $\mathbf{R}_2$  are  $(M_1 + M_2 - 1) \times N$  matrices, and  $\mathbf{R}_s = [\mathbf{r}_s(1), \mathbf{r}_s(2), \dots, \mathbf{r}_s(N)]$ .

#### B. Construction of Virtual Far-Field Data

This section focuses on constructing virtual far-field data in (36), (37) and (38), which enable forming a sparse recovery problem and a phase retrieval formulation for the subsequent estimates of the angle  $\beta_k$  and  $\alpha_k$  in part C of Sec. III, respectively.

First, we construct two covariance matrices as follows

$$\begin{aligned}\mathbf{R}_{11} &= \mathbb{E}\{\mathbf{R}_1\mathbf{R}_1^H\} \\ &= \mathbb{E}\{\mathbf{B}_1\Phi\mathbf{R}_s\mathbf{R}_s^H\Phi^*\mathbf{B}_1^H\} \\ &= \mathbf{B}_1\mathbf{R}_{ss}\mathbf{B}_1^H\end{aligned}\quad (32)$$

$$\begin{aligned}\mathbf{R}_{12} &= \mathbb{E}\{\mathbf{R}_1\mathbf{R}_2^H\} \\ &= \mathbb{E}\{\mathbf{B}_1\Phi\mathbf{R}_s\mathbf{R}_s^H\Phi\mathbf{B}_2^H\} \\ &= \mathbf{B}_1\Phi^2\mathbf{R}_{ss}\mathbf{B}_2^H\end{aligned}\quad (33)$$

where  $\Phi^2$  is the square of matrix  $\Phi$ , and  $\mathbf{R}_{ss} = \mathbb{E}\{\mathbf{R}_s\mathbf{R}_s^H\} = \text{diag}([\sigma_1^2, \sigma_2^2, \dots, \sigma_K^2])$  is a diagonal matrix. The  $k$ th diagonal element of  $\mathbf{R}_{ss}$  is the power of the  $k$ th incident source.

Second, by vectorizing  $\mathbf{R}_{11}$  and  $\mathbf{R}_{12}$ , we have

$$\begin{aligned}\tilde{\mathbf{r}}_{11} &= \text{vec}(\mathbf{R}_{11}) \\ &= (\mathbf{B}_1^* \odot \mathbf{B}_1)\text{undiag}(\mathbf{R}_{ss}) \\ &= \tilde{\mathbf{B}}_{11}\text{undiag}(\mathbf{R}_{ss})\end{aligned}\quad (34)$$

$$\begin{aligned}\tilde{\mathbf{r}}_{12} &= \text{vec}(\mathbf{R}_{12}) \\ &= (\mathbf{B}_2^* \odot \mathbf{B}_1)\text{undiag}(\Phi^2) \\ &= \tilde{\mathbf{B}}_{21}\text{undiag}(\Phi^2\mathbf{R}_{ss})\end{aligned}\quad (35)$$

where  $\tilde{\mathbf{B}}_{11} = [\tilde{\mathbf{b}}_{11}(\omega_{1y}), \tilde{\mathbf{b}}_{11}(\omega_{2y}), \dots, \tilde{\mathbf{b}}_{11}(\omega_{Ky})]$  with  $\tilde{\mathbf{b}}_{11}(\omega_{ky}) = \mathbf{b}_1^*(\omega_{ky}) \odot \mathbf{b}_1(\omega_{ky})$ , and  $\tilde{\mathbf{B}}_{21} = [\tilde{\mathbf{b}}_{21}(\omega_{1y}), \tilde{\mathbf{b}}_{21}(\omega_{2y}), \dots, \tilde{\mathbf{b}}_{21}(\omega_{Ky})]$  with  $\tilde{\mathbf{b}}_{21}(\omega_{ky}) = \mathbf{b}_2^*(\omega_{ky}) \odot \mathbf{b}_1(\omega_{ky})$ . However, the column vectors  $\tilde{\mathbf{r}}_{11}$  and  $\tilde{\mathbf{r}}_{12}$  contain numerous redundant elements, necessitating a process of redundancy removal and reordering, after which we have

$$\bar{\mathbf{r}}_{11} = \bar{\mathbf{B}}_{11}\text{undiag}(\mathbf{R}_{ss})\quad (36)$$

$$\bar{\mathbf{r}}_{12} = \bar{\mathbf{B}}_{21}\text{undiag}(\Phi^2\mathbf{R}_{ss})\quad (37)$$

where  $\bar{\mathbf{B}}_{11} = [\bar{\mathbf{b}}_{11}(\omega_{1y}), \bar{\mathbf{b}}_{11}(\omega_{2y}), \dots, \bar{\mathbf{b}}_{11}(\omega_{Ky})]$  with  $\bar{\mathbf{b}}_{11}(\omega_{ky}) = [e^{-2j\Omega_{3,1}\omega_{ky}}, e^{-2j\Omega_{3,2}\omega_{ky}}, \dots, e^{-2j\Omega_{3,n_1}\omega_{ky}}]^T$ , and  $\bar{\mathbf{B}}_{21} = [\bar{\mathbf{b}}_{21}(\omega_{1y}), \bar{\mathbf{b}}_{21}(\omega_{2y}), \dots, \bar{\mathbf{b}}_{21}(\omega_{Ky})]$  with  $\bar{\mathbf{b}}_{21}(\omega_{ky}) = [e^{-2j\Omega_{4,1}\omega_{ky}}, e^{-2j\Omega_{4,2}\omega_{ky}}, \dots, e^{-2j\Omega_{4,n_2}\omega_{ky}}]^T$ ;  $\Omega_{3,n_1}$  and  $\Omega_{4,n_2}$  represent the  $y$ -coordinate value of the  $n_1$ th element in the virtual array 1 and the  $n_2$ th element in the virtual array 2.

The covariance matrix of  $\bar{\mathbf{r}}_{11}$  can be calculated as follows

$$\mathbf{R} = \mathbb{E}\{\bar{\mathbf{r}}_{11}\bar{\mathbf{r}}_{11}^H\} = \mathbf{\Gamma}\mathbf{T}\mathbf{\Gamma}^H.\quad (38)$$

Here  $\mathbf{T} = \mathbb{E}\{\mathbf{B}\mathbf{A}\mathbf{B}^H\}$  is the Toeplitz matrix, where  $\mathbf{B} = [\mathbf{b}(\omega_{1y}), \mathbf{b}(\omega_{2y}), \dots, \mathbf{b}(\omega_{Ky})]$  with  $\mathbf{b}(\omega_{ky}) = [e^{-2j(-2M_1M_2+M_1+M_2)\omega_{ky}}, e^{-2j(-2M_1M_2+M_1+M_2+1)\omega_{ky}}, \dots, e^{-2j(2M_1M_2-M_1-M_2)\omega_{ky}}]^T$ ,  $\mathbf{A} = \text{undiag}(\mathbf{R}_{ss}) * \text{undiag}(\mathbf{R}_{ss})^H$ ,  $\mathbf{\Gamma}$  is an  $H \times F$  selection matrix,  $H$  is the number of elements in the virtual array 1, and  $F = (4M_1M_2 - 2M_1 - 2M_2 + 1)$ .

### C. Estimation of $\alpha_k$ and $\beta_k$

We now employ SPA<sup>1</sup> [33] to solve the sparse recovery of (39), obtaining the angle  $\beta_k$ , and subsequently apply the phase retrieval operation to determine the angle  $\alpha_k$ .

In order to estimate  $\beta_k$ , SPA is used to recover the Toeplitz matrix  $\mathbf{T}$  in (38) as follows

$$\min_{\mathbf{x}, \mathbf{T}} x + \text{tr}[\mathbf{\Gamma}\mathbf{T}\mathbf{\Gamma}^H]$$

<sup>1</sup>SPA performs parameter estimation in the continuous range based on the well-established covariance fitting criterion and convex optimization, which is suitable for uniform linear and sparse redundant arrays across varying snapshots.

$$\text{s.t.} \quad \begin{bmatrix} x & \bar{\mathbf{r}}_{11}^H \\ \bar{\mathbf{r}}_{11} & \mathbf{\Gamma}\mathbf{T}\mathbf{\Gamma}^H \end{bmatrix} \geq 0.\quad (39)$$

After obtaining Toeplitz matrix  $\mathbf{T}$  through the SDP solver,  $\omega_{ky}$  can be obtained through root-MUSIC [37]. Then,  $\beta_k$  can be derived via the following expression

$$\beta_k = \arccos\left(\frac{\lambda\omega_{ky}}{-2\pi d}\right).\quad (40)$$

Leveraging the estimated values of  $\beta_k$ , we construct matrix  $\bar{\mathbf{B}}_{21}$  based on the formulation of vector  $\bar{\mathbf{b}}_{21}(\omega_{ky})$ . Then, applying the pseudo-inverse of  $\bar{\mathbf{B}}_{21}$  to (37),  $\text{undiag}(\Phi^2\mathbf{R}_{ss})$  is obtained as bellow

$$\text{undiag}(\Phi^2\mathbf{R}_{ss}) = (\bar{\mathbf{B}}_{21})^\dagger \bar{\mathbf{r}}_{12}.\quad (41)$$

According to (26), it follows that  $\omega_{kx}$  can be derived from the estimated matrix  $\Phi$ . Similar to (40),  $\alpha_k$  is derived by

$$\alpha_k = \arccos\left(\frac{\text{angle}(\text{undiag}(\Phi^2\mathbf{R}_{ss})_k)/2}{-2\pi d/\lambda}\right).\quad (42)$$

It is noteworthy that, owing to the phase retrieval operation, automatic pairing between angles  $\alpha$  and  $\beta$  is achieved.

### D. Estimation of $r_k$

In this section, we perform cross-correlation calculation between the data in (11)-(12) and that from the coordinate system's origin in (13), followed by applying the MUSIC algorithm to ultimately derive the range  $r_k$ .

First, we concatenate all elements in subarray 1 and subarray 2 to obtain  $\mathbf{x}(t)$

$$\mathbf{x}(t) = \begin{bmatrix} \mathbf{x}_1(t) \\ \mathbf{x}_2(t) \end{bmatrix} = \begin{bmatrix} \mathbf{A}_1 \\ \mathbf{A}_2 \end{bmatrix} \mathbf{s}(t) + \begin{bmatrix} \mathbf{n}_1(t) \\ \mathbf{n}_2(t) \end{bmatrix} = \mathbf{A}\mathbf{s}(t) + \mathbf{n}(t)\quad (43)$$

where  $\mathbf{A}$  is the steering matrix for  $\mathbf{x}(t)$ , and  $\mathbf{n}(t)$  denotes the additive white Gaussian noise vector of the combined array.

Second, the two types of cross-correlation matrices of  $\mathbf{x}(t)$  and the sensor set at origin are constructed as follows

$$\begin{aligned}\mathbf{r}_z(\tau) &= \mathbb{E}\{\mathbf{x}(t+\tau)\mathbf{x}_3^H(t)\} \\ &= \mathbf{A}_z\mathbf{r}_s(\tau)\end{aligned}\quad (44)$$

$$\begin{aligned}\mathbf{r}_z(-\tau) &= \mathbb{E}\{\mathbf{x}(t)\mathbf{x}_3^H(t+\tau)\} \\ &= \mathbf{A}_z\mathbf{r}_s(-\tau)\end{aligned}\quad (45)$$

where  $\mathbf{x}_3 = [x_3(t), x_3(t), \dots, x_3(t)]^T$  is a  $(2M_1 + 2M_2 - 2) \times 1$  vector. Given  $\mathbf{r}_s(\tau) = \mathbf{r}_s^*(-\tau)$ ,  $\mathbf{r}_z^*(-\tau)$  can be expressed as follows

$$\begin{aligned}\mathbf{r}_z^*(-\tau) &= (\mathbf{A}_z\mathbf{r}_s(-\tau))^* \\ &= \mathbf{A}_z^*\mathbf{r}_s(\tau).\end{aligned}\quad (46)$$

Then, by cascading  $\mathbf{r}_z(\tau)$  and  $\mathbf{r}_z^*(-\tau)$ , we have

$$\bar{\mathbf{r}}_z(\tau) = \begin{bmatrix} \mathbf{r}_z(\tau) \\ \mathbf{r}_z^*(-\tau) \end{bmatrix} = \begin{bmatrix} \mathbf{A}_z \\ \mathbf{A}_z^* \end{bmatrix} \mathbf{r}_s(\tau) = \bar{\mathbf{A}}_z\mathbf{r}_s(\tau)\quad (47)$$

where  $\bar{\mathbf{A}}_z$  is the steering matrix for  $\bar{\mathbf{r}}_z(\tau)$ . Similar to (28) and (29), with  $N$  pseudo snapshots, we have

$$\begin{aligned}\bar{\mathbf{R}}_z &= [\bar{\mathbf{r}}_z(1), \bar{\mathbf{r}}_z(2), \dots, \bar{\mathbf{r}}_z(N)] \\ &= \bar{\mathbf{A}}_z\mathbf{R}_s(\tau)\end{aligned}\quad (48)$$

TABLE I  
ALGORITHM SUMMARY

Steps
Step 1: According to (16) and (17), two types of cross-correlation processing are performed on $\mathbf{x}_1(t)$ and $\mathbf{x}_2(t)$ , resulting in two cross-correlation matrices $\mathbf{R}_1$ and $\mathbf{R}_2$ .
Step 2: Perform covariance calculation on the obtained cross-correlation matrices $\mathbf{R}_1$ and $\mathbf{R}_2$ , followed by vectorization, redundancy removal and reordering operations, to derive $\bar{\mathbf{r}}_{11}$ and $\bar{\mathbf{r}}_{12}$ .
Step 3: Applying the SPA to matrix $\mathbf{R}$ in (38) results in the computation of $\omega_{ky}$ , from which the corresponding $\alpha_k$ and $\beta_k$ are determined based on (40) and (42).
Step 4: Perform cross-correlation between the data of subarray 1 and subarray 2 with the data of the sensor set at origin to obtain matrix $\bar{\mathbf{R}}_z$ , followed by applying the MUSIC method on $\bar{\mathbf{R}}_z$ to derive $r_k$ .

where  $\mathbf{R}_s(\tau) = [\mathbf{r}_s(1), \mathbf{r}_s(2), \dots, \mathbf{r}_s(N)]$ . By constructing matrix  $\bar{\mathbf{A}}_z$  based on estimated 2-D angle parameters and the variable  $r_k$ , and then applying the MUSIC algorithm to  $\bar{\mathbf{R}}_z$ , the estimation of range parameter is achieved.

The proposed algorithm is summarized in TABLE I.

### E. Complexity Analysis

In this part, the complexity of the proposed algorithm and the comparison algorithms is analyzed. Complexity analysis involves considering following aspects: 1) the construction of the virtual array; 2) computation of the covariance matrix; 3) Eigenvalue Decomposition (EVD); 4) spectral peak search; 5) the optimization process. Here, define the search interval of  $\alpha$  as  $\Delta\theta_\alpha$ , the search interval of  $\beta$  as  $\Delta\theta_\beta$ , and the search interval of  $r$  as  $\Delta r$ . Let  $Ran = 2D^2/\lambda - 0.62\sqrt{D^3/\lambda}$  represents the search range, where  $D$  represents array aperture, and  $DoF$  represents the degrees of freedom of the virtual array.  $L$  represents the number of snapshots, and  $M_x$  and  $M_y$  represent the number of elements along the  $x$  and  $y$  coordinates in each algorithm. Then, the complexity of all algorithms is shown in TABLE II.

### F. Discussion

1) Chen's method [32] and Challa's method [38], along with the proposed method all belong to the class of spatial-temporal based NF localization methods. Here we provide the advantages and disadvantages of these three methods. On the one hand, although insensitive to noise, both the compared methods in [32] and [38] resort to fourth-order cumulants to eliminate the range-related quadratic term, while the proposed exploits second-order statistics, which incurs a lower computational complexity to realize 3-D NF localization given a significantly increased number of snapshots, as illustrated in Sec. V-E. On the other hand, under the same number of physical elements, the parameter estimation performance of the proposed algorithm is comparable to that of Chen's method; however, it significantly outperforms Challa's algorithm, offering the ability to perform underdetermined mixed source parameter estimation.

2) In this paper, we employ a sparse recovery method named SPA [33] to estimate the angle  $\beta$ , the angle  $\alpha$  is achieved by a phase retrieval operation, and the range  $r$  using the 1-D MUSIC method. The reason is that in (36) and (37),

TABLE II  
ALGORITHM COMPLEXITY

Algorithm	Complexity
Proposed	$O\{2(M_1 + M_2 - 1)^2N + (4(M_1 + M_2 - 1))^2N + (4(M_1 + M_2 - 1))^3 + K(4(M_1 + M_2 - 1))^2Ran/\Delta r + K^2(DoF)^{2.5} + (DoF)^3 + (4(M_1 + M_2 - 1))^3\}$
TSMUSIC [39]	$O\{9(M_x^2 + M_y^2)L + 9((M_x - 1)/2 + 1)^2L + M_x^3 + M_y^3 + 9((M_y - 1)/2 + 1)^2L + ((M_x - 1)/2 + 1)^3 + ((M_y - 1)/2 + 1)^3 + \pi M_x^2/\Delta\theta_\alpha + \pi M_y^2/\Delta\theta_\beta + M_y^2Ran/\Delta r\}$
Challa [38]	$O\{9((M_x - 1)^2 + (M_y - 1)^2)(L - N)N + 2N((M_x - 1)^2 + (M_y - 1)^2) + (M_x - 1)^6 + (M_y - 1)^6 + K^3\}$
Wu [28]	$O\{9M_xM_yL + M_xM_y^2 + K^3 + L(M_x + M_y)^2TRan/\Delta r\}$
Chen [32]	$O\{9(M_x^2 + M_y^2)(L - N)N + LM_xDoF + (5DoF)^2K + K^2(5DoF)^{2.5} + 2(M_x + M_y)(L - N)N + (2(M_x + M_y))^3 + K(2(M_x + M_y))^2Ran/\Delta r + (2(M_x + M_y))^2N\}$

the vectorized data  $\bar{\mathbf{r}}_{11}$  is a single snapshot, behaving like a coherent data model that cannot directly use the MUSIC algorithm without de-correlation operation. On the contrary, SPA is robust to the coherent signal model, and adopted for the estimate of angle  $\beta$ . For the estimate of angle  $\alpha$ , we use a phase retrieval operation, which is for the purpose of simplicity and convenience. To estimate the range  $r$ , we resort to the original multiple numbers of data of the TPSC array along with its conjugate data, and MUSIC is used which not only offers faster computation but also provides higher precision in the estimated parameters. However, it is possible to solve for  $r$  using the  $l_1$  norm in sparse recovery, which may achieve good estimation performance by reasonable selection of exponential regularization parameters.

3) Subspace or sparse based direction-finding methods based on covariance matrices require those matrices to be calculated in a statistical sense. Considering that the actual number of received data snapshots is finite, in this paper we use maximum likelihood estimation to obtain the second-order statistics based covariance matrix  $\mathbf{R}$  with (38) in the time averaged sense. A higher number of snapshots enhance the precision of the estimated covariance matrix, thereby improving the accuracy of subsequent parameter estimation, while a lower number of snapshots may result in less accurate parameter estimates.

## IV. ANALYSIS OF TPSC ARRAY PERFORMANCE

In order to show the enhanced parameter estimation performance using the designed TPSC array, we will analyze some properties of the TPSC array.

### A. Properties of Virtual Array

According to Sec. III-B, two virtual arrays are generated. We only address virtual array 1 in this part. Therefore, any further mention of virtual array in this section will be in reference to virtual array 1.

*Proposition 1: The virtual array is symmetric about the origin, with range  $[-(2M_1M_2 - M_1 - M_2), (2M_1M_2 - M_1 - M_2)]$ .*

*Proof:* Based on the array model in Fig. 1, since subarray 1 and subarray 2 exhibit centrosymmetry about the origin,

taking subarray 1 as an example, subarray 1 consists of two ULAs, i.e.,

$$\mathbb{S}_1 = \{m_1 M_2, -(M_1 - 1) \leq m_1 \leq 0\} \quad (49)$$

$$\mathbb{S}_2 = \{m_2 M_1, 0 \leq m_2 \leq (M_2 - 1)\} \quad (50)$$

where  $\mathbb{S}_1$  and  $\mathbb{S}_2$  respectively represent the y-coordinate sets of all elements in ULA 1 and ULA 2 of subarray 1,  $M_1 > M_2$ . Therefore, the y-coordinate values set of all elements in subarray 1 can be expressed as

$$\mathbb{S} = \mathbb{S}_1 \cup \mathbb{S}_2. \quad (51)$$

Here, we take into account the scope of virtual arrays across various combination scenarios. Assume that  $l_c = s_1 - s_2$ , where  $l_c$  denotes the y-coordinate values of the elements in the virtual array,  $s_1, s_2 \in \mathbb{S}$ . The various cases can be summarized as follows.

1)  $s_1, s_2 \in \mathbb{S}_1$ : define  $s_1 = m_{1a} M_2$  and  $s_2 = m_{1b} M_2$ , where  $m_{1a}, m_{1b} \in [-(M_1 - 1), 0]$ , and it can be deduced that

$$l_c = s_1 - s_2 = (m_{1a} - m_{1b}) M_2. \quad (52)$$

Evidently, the range of  $m_{1a} - m_{1b}$  is  $[-(M_1 - 1), (M_1 - 1)]$ , and thereby the virtual array is symmetric about the origin. Let  $\mathbb{L}_1$  denotes the set of y-coordinate values of the virtual array elements in this case. The range of  $\mathbb{L}_1$  is  $[-(M_1 - 1) M_2, (M_1 - 1) M_2]$ .

2)  $s_1 \in \mathbb{S}_1, s_2 \in \mathbb{S}_2$ : we have

$$l_c = s_1 - s_2 = m_1 M_2 - m_2 M_1. \quad (53)$$

3)  $s_1 \in \mathbb{S}_2, s_2 \in \mathbb{S}_1$ : we have

$$l_c = s_1 - s_2 = m_2 M_1 - m_1 M_2. \quad (54)$$

By analyzing the expressions derived from (53) and (54), it becomes evident that the  $\mathbb{L}_2$  formed by these two cases is symmetric about the origin. The range of  $\mathbb{L}_2$  is  $[-(2M_1 M_2 - M_1 - M_2), (2M_1 M_2 - M_1 - M_2)]$ .

4)  $s_1, s_2 \in \mathbb{S}_2$ : define  $s_1 = m_{2a} M_1$  and  $s_2 = m_{2b} M_1$ , where  $m_{2a}, m_{2b} \in [0, (M_2 - 1)]$ , and we have

$$l_c = s_1 - s_2 = (m_{2a} - m_{2b}) M_1. \quad (55)$$

In this case, the expression for the y-coordinate values of the virtual array elements is given by  $(m_{2a} - m_{2b}) M_1$ . Given that  $m_{2a} - m_{2b}$  is symmetric about the origin, and  $M_1$  is a constant, the virtual array is symmetric about the origin. Let  $\mathbb{L}_3$  denotes the set of y-coordinate values of the virtual array elements in this case. The range of  $\mathbb{L}_3$  is  $[-(M_2 - 1) M_1, (M_2 - 1) M_1]$ .

To summarize, the set of virtual array elements is  $\mathbb{L} = \mathbb{L}_1 \cup \mathbb{L}_2 \cup \mathbb{L}_3$ . Thus, the virtual array retains symmetry about the origin across all cases, and the range of the virtual array is  $[-(2M_1 M_2 - M_1 - M_2), (2M_1 M_2 - M_1 - M_2)]$ .

**Proposition 2:** *Redundant elements<sup>2</sup> are present within the virtual array.*

*Proof:* The collection of y-coordinate values of actual array elements is denoted as  $\mathbb{S}$ . The crux of the issue lies in demonstrating whether there are any redundant elements derived from the difference between  $s_{11}$  and  $s_{12}$ , where  $s_{11}, s_{12} \in \mathbb{S}$ .

<sup>2</sup>The term 'redundant elements' refers to cases where, in the difference co-array, multiple elements may occupy the same coordinate, resulting in unnecessary duplication.

The y-coordinate values of the array elements in the resultant set are

$$l_c = s_{11} - s_{12} \quad (56)$$

where  $l_c$  represents the y-coordinate value of the element in the resultant set.

It can be inferred that there exists a case where  $s_{11} = -(M_1 - 1) M_2$  and  $s_{12} = -(M_1 - 1) M_2$ , resulting in  $l_c = 0$ . Similarly, when  $s_{11} = (M_2 - 1) M_1$  and  $s_{12} = (M_2 - 1) M_1$ ,  $l_c = 0$  as well. Consequently, the combination of two sets of  $\mathbb{S}$  introduces redundancy.

## B. Design of $M_1$ and $M_2$

Based on the model described in Sec. II, the total number of elements in the TPSC array is  $Q = 2(M_1 + M_2) - 1$ . According to Proposition 1, the range of the virtual array is  $[-(2M_1 M_2 - M_1 - M_2), (2M_1 M_2 - M_1 - M_2)]$ , and  $\xi = (2M_1 M_2 - M_1 - M_2)$ . Therefore, when the total number of elements in the TPSC array is fixed, changing  $M_1$  and  $M_2$  can alter the aperture of the virtual array. Through the following analysis, we determine the configuration of  $M_1$  and  $M_2$  for maximizing the aperture of the virtual array.

Since the total number of elements in the TPSC array is a constant  $Q = 2(M_1 + M_2) - 1$ ,  $w = M_1 + M_2$  is also a constant. Substituting  $w$  into the expression of  $\xi$ , we have

$$\begin{aligned} \xi &= 2M_1(w - M_1) - M_1 - (w - M_1) \\ &= -2\left(M_1 - \frac{w}{2}\right)^2 + \frac{w^2}{2} - w. \end{aligned} \quad (57)$$

The quadratic function  $\xi$  reaches its maximum value at  $M_1 = w/2$ , but due to the unknown parity of  $w$ , further discussion is necessary.

1) If  $w$  is odd, one of  $M_1$  and  $M_2$  is odd while the other is even, then the maximum value of  $\xi$  is attained at  $M_1 = (w + 1)/2$ , with  $M_2 = (w - 1)/2$ . Utilizing an expression involving  $Q$  to represent  $M_1$  and  $M_2$  leads to the derivation of  $M_1 = (Q + 3)/4$  and  $M_2 = (Q - 1)/4$ . In this case, the aperture of the virtual array is

$$D = 2\xi = \frac{Q^2 - 2Q - 7}{4}. \quad (58)$$

2) If  $w$  is even and  $w/2$  is odd, and both  $M_1$  and  $M_2$  are odd, it can be inferred that the maximum value of  $\xi$  is attained at  $M_1 = (w + 4)/2$ , with  $M_2 = (w - 4)/2$ . Utilizing an expression involving  $Q$  to represent  $M_1$  and  $M_2$  leads to the derivation of  $M_1 = (Q + 9)/4$  and  $M_2 = (Q - 7)/4$ . In this case, the aperture of the virtual array is as follows

$$D = 2\xi = \frac{Q^2 - 2Q - 67}{4}. \quad (59)$$

3) If both  $w$  and  $w/2$  are even, and both  $M_1$  and  $M_2$  are even, then the maximum value of  $\xi$  is attained at  $M_1 = (w + 2)/2$ , with  $M_2 = (w - 2)/2$ . Utilizing an expression involving  $Q$  to represent  $M_1$  and  $M_2$  leads to the derivation of  $M_1 = (Q + 5)/4$  and  $M_2 = (Q - 3)/4$ . In this case, the aperture of the virtual array is

$$D = 2\xi = \frac{Q^2 - 2Q - 19}{4}. \quad (60)$$

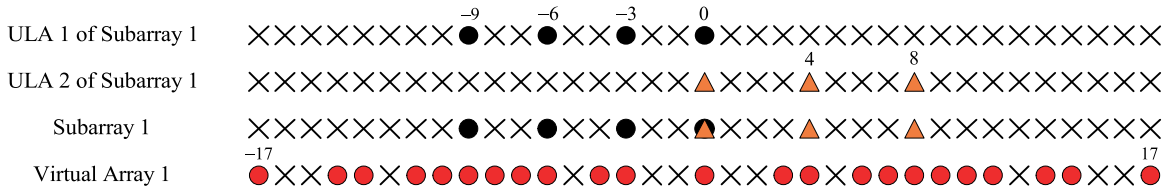
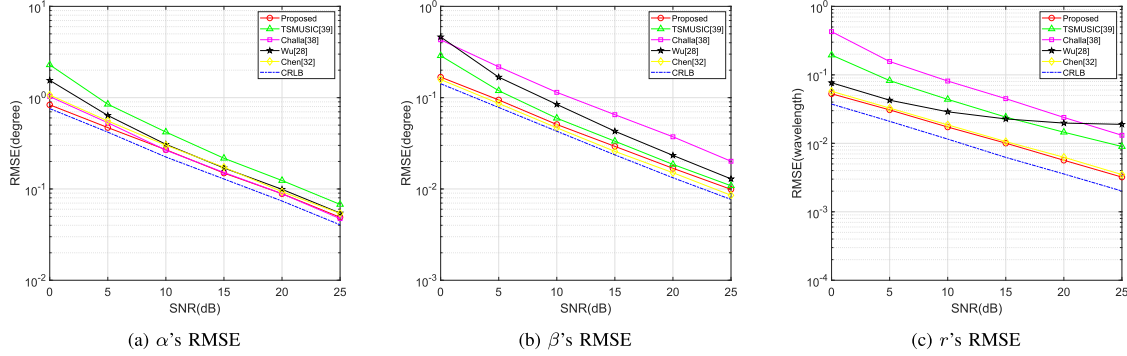
Fig. 3. An array example with  $Q = 13$ .

Fig. 4. RMSE versus SNR.

TABLE III  
OPTIMAL PARAMETER CONFIGURATION FOR TPSC ARRAY

Number of physical elements	$M_1 + M_2$	$(M_1 + M_2)/2$	$M_1$	$M_2$	Aperture of virtual array
$Q = 2(M_1 + M_2) - 1$	Even	Even	$\frac{Q+5}{4}$	$\frac{Q-3}{4}$	$\frac{Q^2-2Q-19}{4}$
		Odd	$\frac{Q+9}{4}$	$\frac{Q-7}{4}$	$\frac{Q^2-2Q-67}{4}$
	Odd		$\frac{Q+3}{4}$	$\frac{Q-1}{4}$	$\frac{Q^2-2Q-7}{4}$

The recommended optimal parameter configuration is detailed in TABLE III. To illustrate the idea of Sec. IV-B, an example is provided in Fig. 3, consisting of a total of  $Q = 13$  elements with  $M_1 = 4$  and  $M_2 = 3$ .

## V. SIMULATION RESULTS

In this section, performance of the proposed algorithm based on the TPSC array is demonstrated and compared with Wu's algorithm [28], Challa's algorithm [38], TSMUSIC [39], and Chen's algorithm [32] as well as the Cramér-Rao lower bound (CRLB) derived in [32]. The impinging non-Gaussian source signals are modelled as  $e^{j\varphi_t}$ , where  $\varphi_t$  is uniformly distributed in  $[0, 2\pi]$ . In the simulations, all sources' power is set to 1. The root mean square error (RMSE) for parameter estimation is defined as follows

$$RMSE = \sqrt{\frac{1}{M_c K} \sum_{i=1}^{M_c} \sum_{j=1}^K (\hat{x}_j^{(i)} - x_j)^2} \quad (61)$$

where  $M_c$  is the number of Monte Carlo runs,  $K$  is the number of sources,  $\hat{x}_j^{(i)}$  denotes the estimation of the  $j$ th signal source during the  $i$ th run, and  $x_j$  is the actual value of the  $j$ th NF source.

### A. RMSE Versus SNR

Fig. 4 shows the RMSE curve versus SNR for different algorithms. The 3-D parameters of the two NF sources are

$(55^\circ, 70^\circ, 1.8\lambda)$  and  $(120^\circ, 117^\circ, 2.3\lambda)$ . The total number of elements of all algorithms is set to 9. TSMUSIC and Wu's algorithm both adopt a symmetric ULA with 3 elements on the x-axis and 7 elements on the y-axis, and Chen's algorithm sets 7 elements on the y-axis with  $M_1 = 3$  and  $M_2 = 2$ , and 3 elements on the x-axis, while for the proposed, we set  $M_1 = 3$  and  $M_2 = 2$ . Given that Challa's algorithm requires an even number of elements along both axes, the simulation has been configured with 4 elements on the x-axis and 6 elements on the y-axis. The total number of snapshots is 1000, while the number of pseudo snapshots of the proposed algorithm, Chen's algorithm, and Challa's algorithm is set to 50. The SNR ranges from 0 to 25dB. The number of Monte Carlo trials is 500.

As illustrated in Fig. 4, the proposed algorithm significantly outperforms the comparison algorithms for angle  $\alpha$ , owing to the greater number of virtual elements generated along the x-axis. While for angle  $\beta$ , the proposed algorithm is only slightly behind Chen's algorithm due to its virtual array aperture along the y-axis being  $(4M_1M_2 - 2M_1 - 2M_2)$ , marginally smaller than the virtual array aperture  $(4M_1M_2 - 4M_2)$  along the y-axis produced by Chen's algorithm. For the range parameter, the proposed algorithm is better than Wu's algorithm, Challa's algorithm and TSMUSIC, and similar to Chen's algorithm, as both the proposed algorithm and Chen's algorithm employ the 1-D MUSIC algorithm to determine the range parameter, leading to comparable estimation performance.

### B. RMSE Versus Number of Snapshots

All configurations remain the same as those in Sec. V-A, except for the number of snapshots and SNR. The SNR is set to 5dB, while the number of snapshots varies from 200 to 5000. As depicted in Fig. 5, the proposed algorithm demonstrates superior result for angle  $\alpha$ ; however, its angle  $\beta$  result is slightly worse than Chen's algorithm, while for range parameter it closely aligns with Chen's algorithm. Notably, the RMSE of the 3-D parameters decreases with an increasing number of snapshots, eventually reaching a flat state.

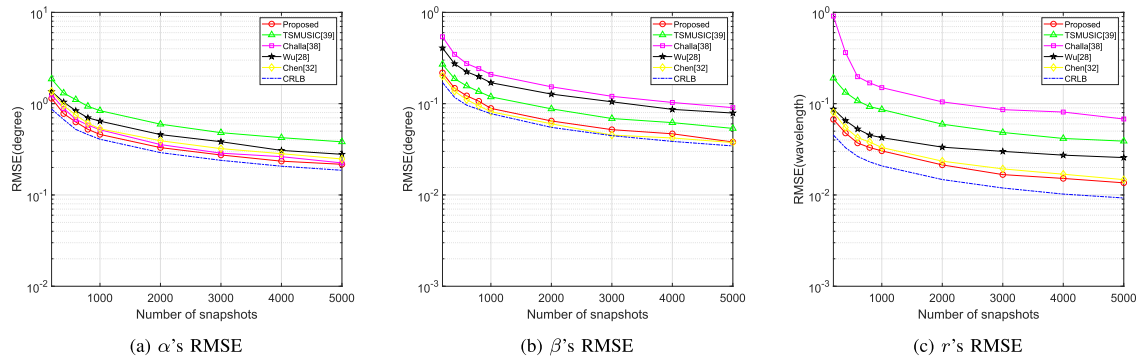


Fig. 5. RMSE versus number of snapshots.

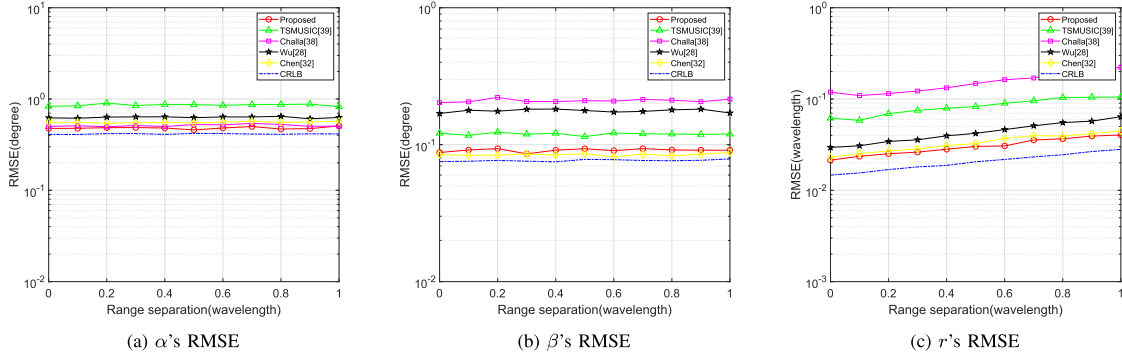


Fig. 6. RMSE versus range separation.

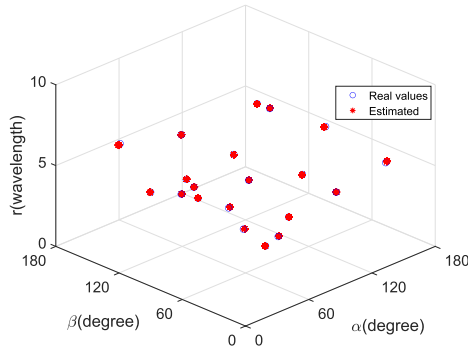
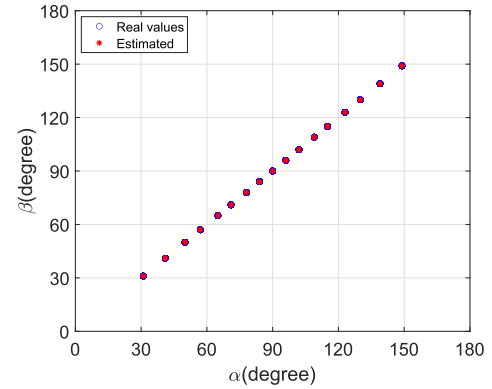


Fig. 7. Locations of the 20 estimated NF sources.



(a) Estimation results of 2-D angles.

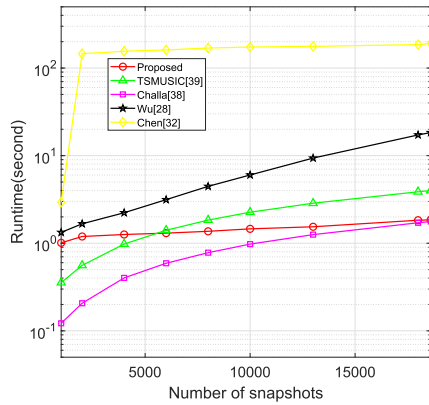
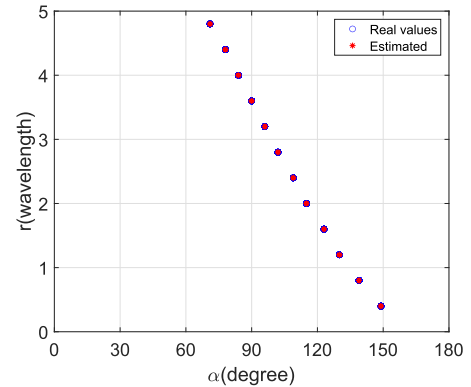


Fig. 8. Runtime comparison.



(b) Estimation results of angle  $\alpha$  and range.

Fig. 9. Parameters estimation in mixed-source scenarios.

C. RMSE Versus Range Separation

In this part, we investigate the impact of range separation on the performance. The parameters are the same as in Sec. V-A except for the range parameter and SNR. The SNR is

set to 5dB, and the first range parameter is set as  $1.8\lambda$ . Initially, the second range parameter is identical to the first,

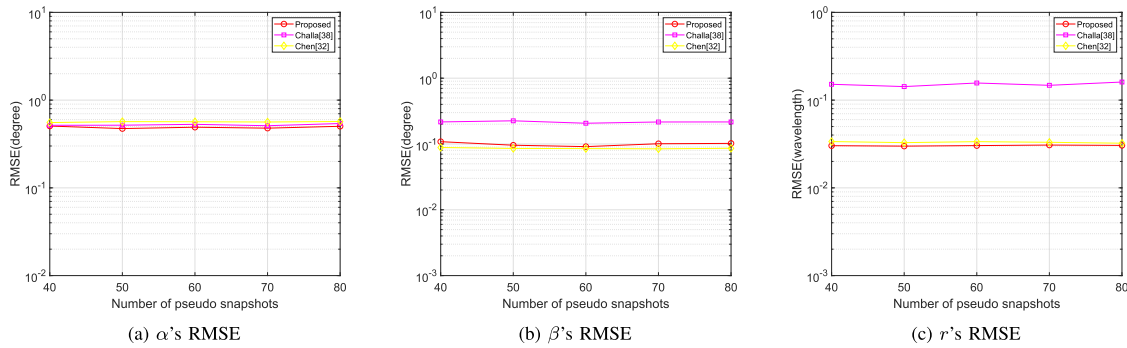


Fig. 10. RMSE versus number of pseudo snapshots.

and the range separation  $\Delta\lambda$  of the second source varies from 0 to  $1\lambda$ . As shown in Fig. 6, the estimation performance for 2-D angle parameters is minimally influenced by range separation, while the range parameter estimation result gets worse with increasing range separation. The reason is that, with the increase of range separation, the second range gets closer to that of an FF source, affecting the accuracy in range estimation.

#### D. Underdetermined Case

In this part, the underdetermined case is considered with 20 NF signals incident on the array, characterized by  $(51^\circ, 112^\circ, 3.7\lambda)$ ,  $(66^\circ, 77^\circ, 6.7\lambda)$ ,  $(56^\circ, 117^\circ, 7.1\lambda)$ ,  $(96^\circ, 42^\circ, 5.6\lambda)$ ,  $(113^\circ, 90^\circ, 7.9\lambda)$ ,  $(83^\circ, 139^\circ, 3.0\lambda)$ ,  $(60^\circ, 29^\circ, 3.1\lambda)$ ,  $(105^\circ, 154^\circ, 1.5\lambda)$ ,  $(147^\circ, 14^\circ, 5.7\lambda)$ ,  $(61^\circ, 63^\circ, 2.6\lambda)$ ,  $(134^\circ, 48^\circ, 3.3\lambda)$ ,  $(78^\circ, 59^\circ, 1.2\lambda)$ ,  $(109^\circ, 68^\circ, 1.9\lambda)$ ,  $(118^\circ, 107^\circ, 7.6\lambda)$ ,  $(47^\circ, 92^\circ, 4.1\lambda)$ ,  $(78^\circ, 94^\circ, 2.6\lambda)$ ,  $(137^\circ, 134^\circ, 1.6\lambda)$ ,  $(141^\circ, 65^\circ, 6.7\lambda)$ ,  $(35^\circ, 125^\circ, 3.9\lambda)$ ,  $(37^\circ, 156^\circ, 6.0\lambda)$ . The TPSC array comprises a total of 17 elements with  $M_1 = 5$  and  $M_2 = 4$ . The SNR is set to 30dB. The number of snapshots is 5000 with the number of pseudo snapshots being 100. The number of Monte Carlo trials is 100. The results are shown in Fig. 7. It can be observed that all 20 NF sources have been distinguished successfully, showing that the proposed algorithm remains effective in underdetermined case.

#### E. Runtime Comparison

In this part, the runtime of each algorithm is compared. The simulation parameters are set the same as in Sec. V-B, except for the number of snapshots which varies from 1000 to 18600. The result is shown in Fig. 8. It can be observed that the runtime of the proposed algorithm is lower than Wu's algorithm and Chen's algorithm. When the number of snapshots is under 6000, the proposed algorithm takes longer time to run than TSMUSIC; however, as the number of snapshots increases beyond 6000, it achieves better runtime performance. This is because TSMUSIC avoids the time-consuming SPA used in our method, making it faster when the number of snapshots is small. However, as the number of snapshots increases, its reliance on fourth-order cumulants slows TSMUSIC down, causing it to perform worse than the proposed algorithm. Although Challa's algorithm is faster for a smaller number of snapshots, its runtime performance declines as the number of snapshots increases significantly, due to higher complexity of

the fourth-order cumulants calculation, which results in longer runtime and ultimately approaches the runtime of the proposed algorithm.

#### F. Mixed Source Scenario

Considering the scenario with mixed NF and FF signals, where all other parameters are the same as those in Sec. V-D except for the signal type. There are 12 NF signals and 5 FF signals, with their parameters given by  $(149^\circ, 149^\circ, 0.4\lambda)$ ,  $(139^\circ, 139^\circ, 0.8\lambda)$ ,  $(130^\circ, 130^\circ, 1.2\lambda)$ ,  $(123^\circ, 123^\circ, 1.6\lambda)$ ,  $(115^\circ, 115^\circ, 2.0\lambda)$ ,  $(109^\circ, 109^\circ, 2.4\lambda)$ ,  $(102^\circ, 102^\circ, 2.8\lambda)$ ,  $(96^\circ, 96^\circ, 3.2\lambda)$ ,  $(90^\circ, 90^\circ, 3.6\lambda)$ ,  $(84^\circ, 84^\circ, 4.0\lambda)$ ,  $(78^\circ, 78^\circ, 4.4\lambda)$ ,  $(71^\circ, 71^\circ, 4.8\lambda)$ ,  $(31^\circ, 31^\circ)$ ,  $(41^\circ, 41^\circ)$ ,  $(50^\circ, 50^\circ)$ ,  $(57^\circ, 57^\circ)$ , and  $(65^\circ, 65^\circ)$ . The results shown in Fig. 9(a) indicate that the angle parameters of all signals are accurately estimated and matched, and all NF signals are localized successfully in Fig. 9(b), thereby demonstrating the proposed algorithm's viability in the mixed-source scenario.

#### G. RMSE Versus Number of Pseudo Snapshots

Finally, we investigate the impact of the number of pseudo snapshots on the performance, where we only consider the delay-based localization methods [32], [38]. All configurations remain the same as those in Sec. V-A, except for the number of pseudo snapshots and SNR. The SNR is set to 5dB, while the number of pseudo snapshots varies from 40 to 80. As shown in Fig. 10, the parameter estimation performance by all the compared methods is barely affected by the varying number of pseudo snapshots.

## VI. CONCLUSION

In this paper, a 3-D parameter estimation algorithm has been proposed for NF sources based on a newly constructed TPSC array. Firstly, leveraging the central symmetry of subarray 1 and subarray 2, two cross-correlation matrices are constructed. Subsequently, by subjecting these matrices to covariance calculation and vectorization, it facilitates the virtual FF transformation of array data, and expanding the virtual array aperture. Following this, 2-D angle estimation is achieved using SPA and a phase retrieval operation. Finally, the range parameter is estimated utilizing the 1-D MUSIC algorithm. Simulation results have demonstrated that the proposed algorithm significantly outperforms the comparison algorithms in terms of estimation accuracy and it can also

effectively deal with underdetermined and mixed-source scenarios.

## REFERENCES

- [1] W. Liu, M. Haardt, M. S. Greco, C. F. Mecklenbräuker, and P. Willett, "Twenty-five years of sensor array and multichannel signal processing: A review of progress to date and potential research directions," *IEEE Signal Process. Mag.*, vol. 40, no. 4, pp. 80–91, Jun. 2023.
- [2] F. Wen, H. Wang, G. Gui, H. Sari, and F. Adachi, "Polarized intelligent reflecting surface aided 2D-DOA estimation for NLoS sources," *IEEE Trans. Wireless Commun.*, vol. 23, no. 7, pp. 8085–8098, Jul. 2024.
- [3] L. Wan, K. Liu, Y. Liang, and T. Zhu, "DOA and polarization estimation for non-circular signals in 3-D millimeter wave polarized massive MIMO systems," *IEEE Trans. Wireless Commun.*, vol. 20, no. 5, pp. 3152–3167, May 2021.
- [4] X. Wu, Z. Yang, Z. Wei, and Z. Xu, "Direction-of-Arrival estimation for constant modulus signals using a structured matrix recovery technique," *IEEE Trans. Wireless Commun.*, vol. 23, no. 4, pp. 3117–3130, Apr. 2024.
- [5] J. He, Y. Wang, T. Shu, and T.-K. Truong, "Polarization, angle, and delay estimation for tri-polarized systems in multipath environments," *IEEE Trans. Wireless Commun.*, vol. 21, no. 8, pp. 5828–5841, Aug. 2022.
- [6] H. Chen et al., "Near-field target localization for EMVS-MIMO radar with arbitrary configuration," *IEEE Trans. Aerosp. Electron. Syst.*, vol. 60, no. 4, pp. 5406–5417, Aug. 2024.
- [7] S. Yang, X. Chen, Y. Xiu, W. Lyu, Z. Zhang, and C. Yuen, "Performance bounds for near-field localization with widely-spaced multi-subarray mmWave/THz MIMO," *IEEE Trans. Wireless Commun.*, vol. 23, no. 9, pp. 10757–10772, Sep. 2024.
- [8] J. He, L. Li, T. Shu, and T.-K. Truong, "Mixed near-field and far-field source localization based on exact spatial propagation geometry," *IEEE Trans. Veh. Technol.*, vol. 70, no. 4, pp. 3540–3551, Apr. 2021.
- [9] X. Wu, C. You, J. Li, and Y. Zhang, "Near-field beam training: Joint angle and range estimation with DFT codebook," *IEEE Trans. Wireless Commun.*, vol. 23, no. 9, pp. 11890–11903, Sep. 2024.
- [10] C. Weng, X. Guo, and Y. Wang, "Near-field beam training with hierarchical codebook: Two-stage learning-based approach," *IEEE Trans. Veh. Technol.*, vol. 73, no. 9, pp. 14003–14008, Sep. 2024.
- [11] X. Zhang, H. Zhang, and Y. C. Eldar, "Near-field sparse channel representation and estimation in 6G wireless communications," *IEEE Trans. Commun.*, vol. 72, no. 1, pp. 450–464, Jan. 2024.
- [12] S. Yang, C. Xie, W. Lyu, B. Ning, Z. Zhang, and C. Yuen, "Near-field channel estimation for extremely large-scale reconfigurable intelligent surface (XL-RIS)-Aided wideband mmWave systems," *IEEE J. Sel. Areas Commun.*, vol. 42, no. 6, pp. 1567–1582, Jun. 2024.
- [13] A. M. Elbir, W. Shi, A. K. Papazafeiropoulos, P. Kourtessis, and S. Chatzinotas, "Near-field terahertz communications: Model-based and model-free channel estimation," *IEEE Access*, vol. 11, pp. 36409–36420, 2023.
- [14] B. Wang, Y. Zhao, and J. Liu, "Mixed-order MUSIC algorithm for localization of far-field and near-field sources," *IEEE Signal Process. Lett.*, vol. 20, no. 4, pp. 311–314, Apr. 2013.
- [15] S. Yang, S. Gao, G. Cui, L. Kong, T. Zhang, and J. Yang, "Iterative self-calibration algorithm for near-field source localization," in *Proc. CIE Int. Conf. Radar (RADAR)*, Oct. 2016, pp. 1–6.
- [16] Y. Tian, Q. Lian, and H. Xu, "Mixed near-field and far-field source localization utilizing symmetric nested array," *Digit. Signal Process.*, vol. 73, pp. 16–23, Feb. 2018.
- [17] X. Wu and J. Yan, "A second-order statistics-based mixed sources localization method with symmetric sparse arrays," *IEEE Commun. Lett.*, vol. 24, no. 8, pp. 1695–1699, Aug. 2020.
- [18] X. Su, P. Hu, Z. Liu, T. Liu, B. Peng, and X. Li, "Mixed near-field and far-field source localization based on convolution neural networks via symmetric nested array," *IEEE Trans. Veh. Technol.*, vol. 70, no. 8, pp. 7908–7920, Aug. 2021.
- [19] Z. Zheng, M. Fu, W.-Q. Wang, and H. C. So, "Symmetric displaced coprime array configurations for mixed near- and far-field source localization," *IEEE Trans. Antennas Propag.*, vol. 69, no. 1, pp. 465–477, Jan. 2021.
- [20] J. Zhang, Y. Li, J. Qi, and Y. Li, "Symmetric extended nested array for passive localization of mixture near- and far-field sources," *IEEE Trans. Circuits Syst. II, Exp. Briefs*, vol. 70, no. 3, pp. 1244–1248, Mar. 2023.
- [21] Y. Tian, X. Wang, X. Jin, and Y. Hou, "Near-field source location estimation algorithm based on coprime array," in *Proc. IEEE Int. Conf. Signal Process., Commun. Comput. (ICSPCC)*, Oct. 2022, pp. 1–5.
- [22] Z. Zheng, Y. Huang, W.-Q. Wang, and H. C. So, "Augmented covariance matrix reconstruction for DOA estimation using difference coarray," *IEEE Trans. Signal Process.*, vol. 69, pp. 5345–5358, 2021.
- [23] J. He, T. Shu, L. Li, and T.-K. Truong, "Mixed near-field and far-field localization and array calibration with partly calibrated arrays," *IEEE Trans. Signal Process.*, vol. 70, pp. 2105–2118, 2022.
- [24] C. Zhou, Y. Gu, Z. Shi, and M. Haardt, "Structured Nyquist correlation reconstruction for DOA estimation with sparse arrays," *IEEE Trans. Signal Process.*, vol. 71, pp. 1849–1862, Mar. 2023.
- [25] X. Dong, J. Zhao, M. Sun, X. Zhang, and Y. Wang, "A modified d-Generalized labeled multi-Bernoulli filtering for multi-source DOA tracking with coprime array," *IEEE Trans. Wireless Commun.*, vol. 22, no. 12, pp. 9424–9437, Dec. 2023.
- [26] Z. Tan, Y. C. Eldar, and A. Nehorai, "Direction of arrival estimation using co-prime arrays: A super resolution viewpoint," *IEEE Trans. Signal Process.*, vol. 62, no. 21, pp. 5565–5576, Nov. 2014.
- [27] R. Cohen and Y. C. Eldar, "Sparse array design via fractal geometries," *IEEE Trans. Signal Process.*, vol. 68, pp. 4797–4812, 2020.
- [28] X. Wu and J. Yan, "3-D mixed far-field and near-field sources localization with cross array," *IEEE Trans. Veh. Technol.*, vol. 69, no. 6, pp. 6833–6837, Jun. 2020.
- [29] Z. Ma, D. He, X. Chen, and W. Yu, "Localization of 3-D near-field sources based on the joint phase interferometer and MUSIC algorithm," in *Proc. IEEE Globecom Workshops (GC Wkshps)*, Dec. 2020, pp. 1–6.
- [30] X. Wu, J. Wang, Y. Liu, and J. Li, "A near-field source localization method for uniform/sparse centrally symmetric rectangular arrays," in *Proc. IEEE Int. Conf. Acoust., Speech Signal Process. (ICASSP)*, Apr. 2024, pp. 13111–13115.
- [31] J. Fang, J. Liu, H. Chen, W. Liu, Y. Tian, and G. Wang, "Three-dimensional spatial-temporal near-field passive localization based on an exact spatial propagation model," in *Proc. IEEE Int. Conf. Acoust., Speech Signal Process. (ICASSP)*, Apr. 2024, pp. 8516–8520.
- [32] H. Chen et al., "Spatial-temporal-based underdetermined near-field 3-D localization employing a nonuniform cross array," *IEEE J. Sel. Topics Signal Process.*, vol. 18, no. 4, pp. 561–571, May 2024.
- [33] Z. Yang, L. Xie, and C. Zhang, "A discretization-free sparse and parametric approach for linear array signal processing," *IEEE Trans. Signal Process.*, vol. 62, no. 19, pp. 4959–4973, Oct. 2014.
- [34] Y. Cao, T. Lv, Z. Lin, P. Huang, and F. Lin, "Complex ResNet aided DoA estimation for near-field MIMO systems," *IEEE Trans. Veh. Technol.*, vol. 69, no. 10, pp. 11139–11151, Oct. 2020.
- [35] Z. Jiang, H. Chen, W. Liu, Y. Tian, and G. Wang, "Conjugate augmented spatial-temporal near-field sources localization with cross array," in *Proc. IEEE Int. Conf. Acoust., Speech Signal Process. (ICASSP)*, May 2022, p. 5113.
- [36] H. Chen, W. Wang, and W. Liu, "Joint DOA, range, and polarization estimation for rectilinear sources with a COLD array," *IEEE Wireless Commun. Lett.*, vol. 8, no. 5, pp. 1398–1401, Oct. 2019.
- [37] B. D. Rao and K. V. S. Hari, "Performance analysis of root-music," *IEEE Trans. Acoust., Speech, Signal Process.*, vol. 37, no. 12, pp. 1939–1949, Dec. 1989.
- [38] R. N. Challa and S. Shamsunder, "Passive near-field localization of multiple non-Gaussian sources in 3-D using cumulants," *Signal Process.*, vol. 65, no. 1, pp. 39–53, Feb. 1998.
- [39] J. Liang and D. Liu, "Passive localization of mixed near-field and far-field sources using two-stage MUSIC algorithm," *IEEE Trans. Signal Process.*, vol. 58, no. 1, pp. 108–120, Jan. 2010.



**Hua Chen** (Senior Member, IEEE) received the M.Eng. and Ph.D. degrees in information and communication engineering from Tianjin University, Tianjin, China, in 2013 and 2017, respectively. He is currently an Associate Professor with the Faculty of Electrical Engineering and Computer Science, Ningbo University, China. His research interests include array signal processing and MIMO radar. He is an Associate Editor for *Circuits, Systems, and Signal Processing*.



**Junjie Li** received the B.S. degree in communication engineering from Ningbo University, Ningbo, China, in 2024. He is currently pursuing the M.S. degree in integrated circuit engineering with the School of Integrated Circuits, Southeast University. His research interests include electronic design automation.



**Songjie Yang** received the B.E. degree in communication engineering from Shanghai University in 2020. He is currently pursuing the Ph.D. degree with the National Key Laboratory of Wireless Communications, University of Electronic Science and Technology of China. His research interests include near-field sensing and communications, reconfigurable intelligent surfaces, cell-free communications, precoding, channel estimation, and machine learning techniques.



**Wei Liu** (Senior Member, IEEE) received the B.Sc. degree in space physics and the L.L.B. degree in intellectual property law from Peking University, Beijing, China, in 1996 and 1997, respectively, the M.Phil. degree from the Department of Electrical and Electronic Engineering, The University of Hong Kong, Hong Kong, in 2001, and the Ph.D. degree from the School of Electronics and Computer Science, University of Southampton, Southampton, U.K., in 2003.

From 2005 to 2023, he was a Lecturer/a Senior Lecturer at the Department of Electronic and Electrical Engineering, University of Sheffield, Sheffield, U.K., and from 2023 to 2024, a Reader at the School of Electronic Engineering and Computer Science, Queen Mary University of London, London, U.K. Since August 2024, he has been a Professor at the Department of Electrical and Electronic Engineering, The Hong Kong Polytechnic University, Hong Kong. His research interests cover a wide range of topics in signal processing, with a focus on sensor array signal processing and its various applications, such as robotics and autonomous systems, human-computer interface, radar, sonar, and wireless communications. He is a member of the Applied Signal Processing Systems Technical Committee of the IEEE Signal Processing Society (SPS) (from 2023 to 2025), the Digital Signal Processing Technical Committee of the IEEE Circuits and Systems Society (the Chair from 2022 to 2024), and the IEEE SPS Education Board (from 2024 to 2026, the Chair of its Educational Conference Program Committee), and a Former Member of the Sensor Array and Multichannel Signal Processing Technical Committee of the IEEE SPS (the Chair from 2021 to 2022), the IEEE SPS Technical Directions Board (from 2021 to 2022), and the IEEE SPS Conference Board and its Executive Subcommittee (from 2022 to 2023). Currently, he is an Associate Editor of IEEE ANTENNAS AND WIRELESS PROPAGATION LETTERS and IEEE TRANSACTIONS ON CIRCUITS AND SYSTEMS—I: REGULAR PAPERS, and an Executive Associate Editor-in-Chief of the *Frontiers of Information Technology and Electronic Engineering*.



**Yonina C. Eldar** (Fellow, IEEE) received the B.Sc. degree in physics and the B.Sc. degree in electrical engineering from Tel Aviv University, Tel-Aviv, Israel, 1995 and 1996, respectively, and the Ph.D. degree in electrical engineering and computer science from the Massachusetts Institute of Technology (MIT), Cambridge, MA, USA, in 2002. She was a Visiting Professor at Stanford University. She is currently a Professor with the Department of Mathematics and Computer Science, Weizmann Institute of Science, Rehovot, Israel, where she heads the Center for Biomedical Engineering and Signal Processing and holds the Dorothy and Patrick Gorman Professorial Chair. She is also a Visiting Professor at MIT, a Visiting Scientist at the Broad Institute, and an Adjunct Professor at Duke University. She is a member of the Israel Academy of Sciences and Humanities and a EURASIP Fellow. She has received many awards for excellence in research and teaching, including the IEEE Signal Processing Society Technical Achievement Award (2013), the IEEE/AESS Fred Nathanson Memorial Radar Award (2014), and the IEEE Kiyomi Tomiyasu Award (2016). She was a Horev Fellow of the Leaders in Science and Technology Program at the Technion and an Alon Fellow. She received the Michael Bruno Memorial Award from the Rothschild Foundation, the Weizmann Prize for Exact Sciences, the Wolf Foundation Krill Prize for Excellence in Scientific Research, the Henry Taub Prize for Excellence in Research (twice), the Hershel Rich Innovation Award (three times), and the Award for Women with Distinguished Contributions. She received several best paper awards and best demo awards together with her research students and colleagues, was selected as one of the 50 most influential women in Israel, and was a member of the Israel Committee for Higher Education. She is the Editor-in-Chief of *Foundations and Trends in Signal Processing*, a member of several IEEE Technical Committees and Award Committees, and heads the Committee for Promoting Gender Fairness in Higher Education Institutions in Israel.



**Chau Yuen** (Fellow, IEEE) received the B.Eng. and Ph.D. degrees from Nanyang Technological University, Singapore, in 2000 and 2004, respectively.

He was a Post-Doctoral Fellow with Lucent Technologies Bell Labs, Murray Hill, in 2005, and a Visiting Assistant Professor with The Hong Kong Polytechnic University in 2008. From 2006 to 2010, he was with the Institute for Infocomm Research, Singapore. From 2010 to 2023, he was an Associate Professor with the Engineering Product Development Pillar, Singapore University of Technology and Design. Since 2023, he has been with the School of Electrical and Electronic Engineering, Nanyang Technological University.

Dr. Yuen received the IEEE Communications Society Fred W. Ellersick Prize in 2023, the IEEE Marconi Prize Paper Award in Wireless Communications in 2021, the IEEE APB Outstanding Paper Award in 2023, the IEEE ICC Best Paper Award in 2023, and the EURASIP Best Paper Award for *Journal on Wireless Communications and Networking* in 2021. He was also a recipient of the Lee Kuan Yew Gold Medal, the Institution of Electrical Engineers Book Prize, the Institute of Engineering of Singapore Gold Medal, the Merck Sharp and Dohme Gold Medal, and twice a recipient of the Hewlett Packard Prize. He serves as the Editor-in-Chief for *Computer Science* (Springer Nature) and an Editor for IEEE TRANSACTIONS ON VEHICULAR TECHNOLOGY, IEEE SYSTEM JOURNAL, and IEEE TRANSACTIONS ON NETWORK SCIENCE AND ENGINEERING, where he was awarded as IEEE TRANSACTIONS ON NETWORK SCIENCE AND ENGINEERING Excellent Editor Award and a Top Associate Editor for IEEE TRANSACTIONS ON VEHICULAR TECHNOLOGY from 2009 to 2015. He is a Distinguished Lecturer of the IEEE Vehicular Technology Society, Top 2% Scientists by Stanford University, and also a Highly Cited Researcher by Clarivate Web of Science. He has three U.S. patents and published over 500 research papers at international journals or conferences.